MARTIAN IMPACT CRATERS AND THEIR IMPLICATIONS FOR TARGET CHARACTERISTICS

Nadine G. Barlow

Northern Arizona University, Department of Physics and Astronomy, Flagstaff, AZ 86011-6010 USA
Nadine.Barlow@nau.edu

ABSTRACT

Martian impact craters display a number of characteristics which differ from those associated with impact craters on volatile-poor bodies such as the Moon or Mercury. These characteristics include the morphometric properties of the crater, ejecta and interior morphologies, and the range of preservational states due to modification from the Martian environment. Both the thin Martian atmosphere and the presence of volatiles within the target material can contribute to these unusual characteristics, but the role of target volatiles appears to dominates.

1. INTRODUCTION

Lunar impact craters have become the "standard" to which impact craters on other bodies have been compared. However, the Moon is a volatile-poor body, with no substantial atmosphere or presence of volatiles within the target material. The presence of volatiles substantially affects impact craters, both during crater formation and through subsequent modification. Examples of these effects are clearly evident in Martian impact craters, which serve as better analogs to terrestrial craters than do lunar craters.

Martian impact craters were identified in the early imagery from Mariners 4, 6, 7, and 9, but it was not until the Viking missions in the late 1970's that the full range of morphologic features could be appreciated. The latest armada of orbiting spacecraft (Mars Global Surveyor (MGS), Mars Odyssey, and Mars Express (MEx)) has dramatically enhanced the amount of information about Martian impact craters by providing multispectral, stereo, topographic, and mineralogic data. The recent addition of the Mars Reconnaissance Orbiter (MRO) together with in situ analysis of impact crater materials by the Mars Exploration Rovers (MER) are adding additional layers of information to help us better understand how the Martian environment, and particularly the presence of atmospheric and subsurface volatiles, has influenced the formation and subsequent modification of impact craters on our neighboring world. Peering below the surface with MEx's MARSIS and MRO's SHARAD ground penetrating radars will provide direct constraints on the role of subsurface volatiles in producing the observed morphologies and morphometries of Martian impact craters.

2. CRATER MORPHOMETRY

Viking-based analysis of Martian impact craters using shadow measurements and photoclinometry suggested that many of the morphometric parameters were quite different from those of lunar craters [1, 2]. The detailed topographic information produced by MGS's Mars Orbiter Laser Altimeter (MOLA) instrument has confirmed that crater morphometric properties are quite different between Mars and volatile-poor bodies such as the Moon and Mercury [3, 4].

The gravity-dependence of the transition between simple and complex crater forms is well-established, predicting that the simple-to-complex transition diameter (D_{sc}) should be smaller on larger and/or more massive bodies [5]. Gravity scaling predicts that D_{sc} on Mars should be about 10 km, similar to D_{sc} on smaller but more massive Mercury. The actual value for Mars is closer to 7 km, although D_{sc} is observed to be smaller at higher latitudes [3]. These observations suggest that the crust is weakened by the presence of ice within the near-surface materials.

Other morphometric properties also show variations with latitude. For example, the relationship between the depth (d) and the diameter (D) of fresh complex craters [3, 6] at near-polar latitudes is

$$d = 0.03\ D^{1.04} \qquad (1)$$

while the relationship in near-equatorial regions is

$$d = 0.19\ D^{0.55} \qquad (2)$$

Similar latitudinal dependencies are observed for other morphometric parameters (see [3] for more details). These latitudinal variations in crater morphometries are consistent with the proposed latitudinal distribution of near-surface ice, based on geothermal models [7-9].

3. EJECTA MORPHOLOGIES

Fresh lunar impact craters are surrounded by a radially-oriented ejecta blanket, emplaced by dry material ejected along ballistic trajectories. Such ejecta blankets, referred to here as "lunar radial ejecta", are comprised of an inner thick, hummocky deposit called the continuous ejecta blanket surrounded by the more dispersed, secondary crater-dominated discontinuous ejecta blanket [5]. Fresh Martian impact craters, however, are typically surrounded by ejecta blankets displaying a more lobate or fluidized appearance. Such ejecta morphologies are called "layered ejecta", and are subdivided into several classes based on the appearance of the ejecta [10]. Craters displaying one complete layer of ejecta are called single layer ejecta (SLE) craters, while those displaying two complete ejecta layers are double layer ejecta (DLE) craters. Multiple layer ejecta (MLE) craters are surrounded by three or more partial or complete ejecta layers. Two models have been proposed for the formation of the layered ejecta morphologies: (1) vaporization of volatile-rich target material during impact [11, 12], and (2) interaction of the ejecta plume with the thin Martian atmosphere [13, 14].

3.1. Single Layer Ejecta

SLE craters display a single ejecta blanket surrounding the crater (Fig. 1). They are the most common type of ejecta morphology surrounding fresh craters on Mars [15]. The smallest craters which show a SLE morphology (the "onset diameter") range from about 3 to 5 km in the equatorial region to less than 1 km near the poles, although regional variations are seen in the equatorial region [16-18]. The SLE morphology is associated with craters up to about 25 km in diameter in the equatorial region and up to >70-km-diameter near the poles. The ejecta blanket is characterized by two quantitative measurements, the ejecta mobility (EM) ratio and lobateness (Γ), which are believed to provide information about the fluidity of the ejecta during emplacement. The EM ratio describes how far the ejecta extends from the crater and is defined as [19, 20]

$$EM = \frac{\text{(maximum extent of ejecta from crater rim)}}{\text{(crater radius)}} \quad (3)$$

Lobateness is a measure of the sinuosity of the ejecta deposit. It is defined in terms of the area covered by the ejecta (A) and the perimeter (linear distance along outer edge) of the ejecta deposit (P) [21]:

$$\Gamma = P/(4\pi A)^{1/2} \quad (4)$$

A circular ejecta blanket will have Γ = 1 while more sinuous ejecta have higher values. Martian SLE craters have EM ratios between 0.20 and 6.60, with a median of 1.53. Their lobateness values vary from 1.00 to 3.57, with an average of 1.10. Hence, most SLE craters have ejecta deposits which extend ~1.5 crater radii from the rim and which are generally close to circular. EM and Γ values typically indicate more fluid ejecta as one approaches the poles, consistent with the proposed higher concentrations of subsurface volatiles in these regions from geothermal and hydrologic models [8, 9] as well as the observed high hydrogen concentrations from the Gamma Ray Spectrometer/Neutron Spectrometer on Mars Odyssey [22-24].

Both the subsurface volatile [11, 12] and atmospheric [13, 14] models can replicate the general features of the SLE morphology. However, the observed latitudinal variations in onset diameter, EM, and Γ strongly suggest that subsurface volatiles dominate the formation process.

Figure 1. Examples of single layer ejecta (SLE) craters on Mars. Crater on right is 11.6 km in diameter and located at 23.63°N 101.71°E. (THEMIS image I02493005)

3.2 Double Layer Ejecta

DLE craters display two complete ejecta layers (Fig. 2) and are commonly found around craters in the mid-latitude (~40°-65°) zone in both hemispheres. This ejecta morphology is seen around craters up to ~25-km-diameter. Detailed analysis of the DLE ejecta blankets using MGS's Mars Orbiter Camera (MOC) and Odyssey's Thermal Emission Imaging System (THEMIS) visible (VIS) camera suggest that the inner ejecta layer is emplaced before the outer layer [25]. Contrary to earlier reports, DLE craters are seen at a range of elevations and in materials with varying

thermal inertia values [15, 26], but they are most strongly concentrated in low-lying regions of the northern hemisphere between 40°N and 65°N.

EM ratios vary from 0.40 to 3.30 for the inner ejecta layer, with an average value of 1.49. The outer ejecta layer has an EM range of 1.20 to 10.60 with an average of 3.24 [27]. Thus the outer ejecta layer displays much greater fluidity than the inner layer, which is similar in its EM values to those of SLE craters. The outer layer also displays high lobateness values, ranging from 1.01 to 2.27 with an average of 1.14. Inner layer Γ ranges between 1.00 and 1.38, with an average of 1.04.

The high EM and Γ values, as well as onset diameters of <1 km and concentrations within latitude zones expected to be ice-rich, all suggest that target volatiles are responsible for the DLE morphology. The inner layer displays many characteristics which are similar to those of SLE craters in these same regions and likely form by a similar mechanism. The very high EM ratios for the outer layers may indicate interaction of the ejecta plume with the Martian atmosphere, such as through a base surge process [25].

Figure 2: This double layer ejecta (DLE) crater is 6.8 km in diameter and located at 46.7°N 325.7°E. (THEMIS image I03484002)

3.3. Multiple Layer Ejecta Craters

The MLE morphology is most commonly associated with craters in the 25-50-km-diameter range, although craters as small as 8-km-diameter can show this ejecta pattern. Multiple layer craters display three or more ejecta layers which can extend completely around the crater or only as partial segments (Fig. 3). Most MLE craters are concentrated along the highlands/lowlands dichotomy boundary [15].

Analogous to the outer layer of DLE craters, the outermost complete ejecta deposit of the MLE craters has very high EM and Γ values, indicating that the

ejected material was very fluid at the time of emplacement. EM ratios range from 0.30 to 4.70, with an average value of 2.17; lobateness has an average value of 1.18 with a range of 1.02 to 1.74 [27].

The generally large size of MLE craters suggests that they are excavating to depths of around 1 km or more, within the regions where groundwater reservoirs could exist based on geothermal models [8, 9]. Both incorporation of liquid water within the ejected material [28] and interaction of the vapor plume with the Martian atmosphere [27] have been proposed to explain the extreme fluidity of the MLE ejecta deposits.

Figure 3: Multiple layer ejecta (MLE) craters display 3 or more partial or complete ejecta layers. This 25 km MLE crater at 6°N 304°E also displays a summit pit. (THEMIS image I03218002)

3.4. Other Ejecta Morphologies

The SLE, DLE, and MLE morphologies constitute 89% of all the ejecta morphologies associated with Martian impact craters ≥5-km-diameter [27]. Although the other ejecta morphologies are numerically minor, the size and regional distributions of these features provide additional insights into the properties of the target materials.

Very small (typically <3-km-diameter in the equatorial region) and very large (typically >50-km-diameter) craters often display a radial (Rd) ejecta pattern, which

is qualitatively similar to the lunar radial ejecta patterns (Figure 4). Secondary crater chains are common in this ejecta pattern and can extend for 100's of crater radii from the crater rim [29]. This has led some researchers to conclude that the small crater population (<1-km-diameter) is dominated by secondary craters, which has important implications for terrain ages derived from small crater statistics.
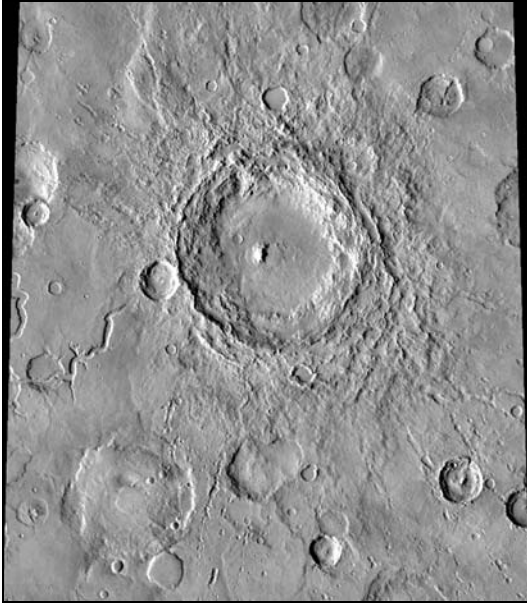

Figure 4: Radial (Rd) ejecta craters, like this 114-km-diameter example, show little or no evidence of ejecta fluidization, but chains of secondary craters are obvious. Crater is located at 32.14°N 21.99°E. (Viking mosaic image)

Diverse (Di) ejecta display components of both layered and radial ejecta patterns. Typically, chains of secondary craters extend from beneath the outer edge of the layered ejecta deposit (Fig. 5), indicating that the secondary craters are emplaced before the layered deposit. This suggests that volatile-poor but coherent target material is excavated before the volatile-rich region is encountered. The onset diameter for Di ejecta craters varies with age of the surface: Craters on young, Amazonian-aged volcanic lava flows show the Di pattern for craters as small as 10-km-diameter. Intermediate-aged Hesperian surfaces require craters to be at least 19 km in diameter before the Di pattern is seen, and craters on the old Noachian-aged surface are at least 45 km in diameter before showing this ejecta morphology [30]. This diameter-terrain age relationship likely reflects the varying thickness of a weak, fragmented regolith, which would be thicker on older units. Excavation through this thicker regolith to an underlying coherent bedrock layer, necessary for production of the blocks responsible for secondary crater formation, requires a larger crater.
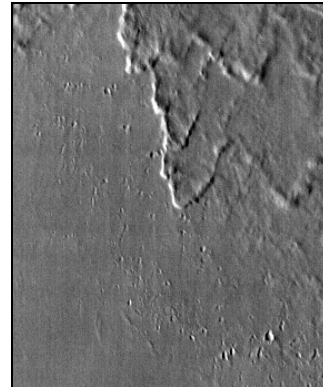

Figure 5: Example of a diverse (Di) ejecta morphology, with small secondary craters extending beyond the outer edge of the multiple layer ejecta blanket. This crater is located at 23.19°N 207.76°E (THEMIS image V01990003)

Pancake (Pn) ejecta craters are associated with ejecta deposits where the outer edge drops off in a convex shape rather than terminating in a distal rampart (Fig. 6). This morphology is primarily seen around craters <20-km-diameter at the higher latitudes, usually in the same 40-65° latitude zone where DLE craters dominate. Costard [20] suggested that Pn craters were simply the inner layer of a double layer crater where the thin outer ejecta layer had been either destroyed or was below detection limits. A more recent analysis of these craters using MOC and THEMIS data supports this idea [26]. Not only are many craters classified as Pn craters using Viking imagery found to actually be DLE craters using higher resolution data, but the EM and Γ values for Pn craters are statistically identical to the inner layer of DLE craters.
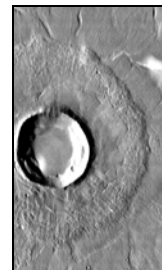

Figure 6: Pancake (Pn) craters do not display a terminal ridge (rampart) to their ejecta deposits. Crater is 14.1 km in diameter and located at 34.90°N 102.58°E. Higher resolution suggests this is actually a degraded DLE crater (THEMIS image I04378002)

Pedestal (Pd) craters are an unusual landform where both the crater and ejecta blanket are elevated above the surrounding terrain (Fig. 7). Pd craters are very small (typically <5-km-diameter) and are concentrated in the 45-60° latitude zone in both hemispheres. The original explanation for these features was that eolian deflation of surrounding fine-grained materials left the crater and ejecta blanket perched above the surroundings. However, Pd craters tend to be found within the ice-rich fine-grained mantles proposed to be deposited during high obliquity periods. A new model has been proposed by which sublimation of the ice within this mantling material causes the lowering of the surrounding terrain and the perched characteristics of the Pd craters [26].
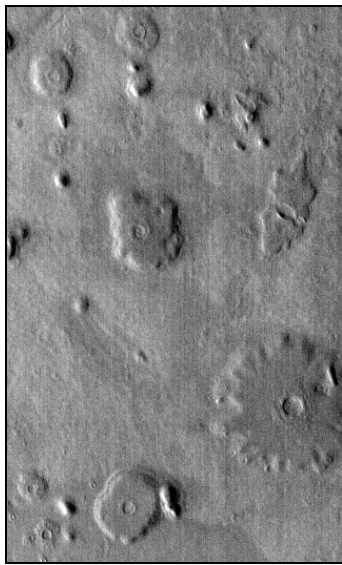

Figure 7: Pedestal (Pd) craters often occur in clusters, as seen in this image from the Arcadia Planitia region of Mars. The largest crater (lower right) is 1.8 km in diameter and located near 42.4°N 154.6°E. (THEMIS image I11416010)

4. INTERIOR MORPHOLOGIES

Martian impact craters display a variety of interior morphologies, including central peaks, peak rings, flat floors, and wall terraces. Collapse pits are seen on the floors of some craters while others have their floors covered with sedimentary deposits of eolian or possibly lacustrine origin. One class of interior features which is common on Mars but absent on volatile-poor bodies like the Moon are central pits.

4.1. Central Pits

Central pits are depressions found in the center of crater floors. There are two types of central pits: floor pits, where the pit lies directly on the floor of the crater, and summit pits, where the pit is found on a central rise or on top of a central peak. Fig. 8 shows an example of a floor pit while a summit pit is seen in Fig. 3. Over 1500 central pit craters have been identified on Mars, with floor pits approximately twice as common as summit pits [31]. Both floor pits and summit pits are found in craters with a similar range in sizes (5 to 57 km in diameter) and over a similar latitude zone (50°N to 70°S). The ratio of the pit diameter to the crater diameter (D_p/D_c) is strongly peaked for floor pits near 0.15 (range: 0.07 to 0.29). Summit pits tend to be smaller relative to their parent crater than floor pits (median = 0.11), but are not as strongly peaked over the range of 0.05 to 0.19 (Fig. 9). Pit craters are found in craters with a wide range in preservational state, from very degraded to pristine. Among fresh craters with preserved ejecta morphologies, most display a multiple layer ejecta morphology.
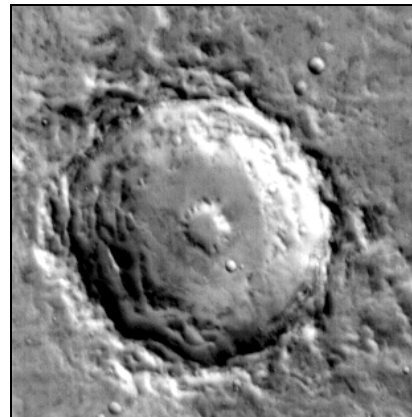

Figure 8: This 20.7-km-diameter crater displays a central floor pit. Crater is located at 22.46°N 340.41°E. (THEMIS image I01199005)

Central pits are believed to result from the release of volatiles from the center of the crater during crater formation. Croft [32] suggested that this resulted from cometary impacts, but the lack of central pit craters on volatile-poor bodies such as the Moon and Mars argues against central pits being solely a result of impactor composition. Because central pit craters are also common on icy moons such as Ganymede [33, 34] and Europa [35], the most widely accepted model of central pit formation involves impact into volatile-rich target materials [36]. Recent numerical modeling of both asteroid and comet impacts into ice-soil mixed targets shows that temperatures within the central region of the

transient cavity can reach temperatures well above the vaporization point of water ice [37]. A sudden release of this vapor could be responsible for the formation of central pits. The fact that craters in a wide range of preservational states (and thus a range of ages) display central pits suggests that the target volatiles responsible for central pit formation have been present on Mars for most if not all of its history.
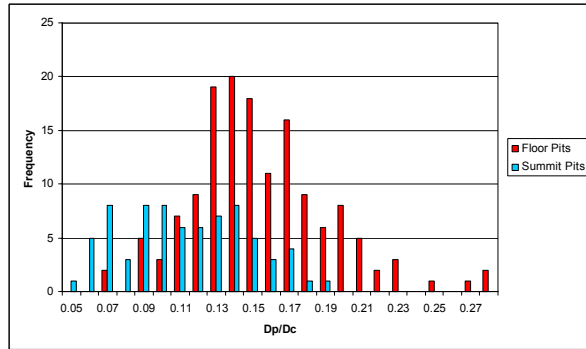

Figure 9: Comparison of D_p/D_c values for floor and summit pits. Floor pits show a stronger peak and tend to be larger relative to their parent crater than summit pits.

Major questions which still remain for central pits are: (1) why are some pits found on crater floors while others occur on top of central rises, and (2) why do some craters display central pits when adjacent craters of similar size and age do not? An on-going study to compare central pit craters on Ganymede with their Martian analogs may help to resolve these questions [38].

5. DEGRADATION OF MARTIAN CRATERS

While the layered ejecta morphologies and central pits strongly suggest the presence of volatiles in the target material at the time of crater formation, a number of processes related to volatiles operate to modify Martian impact craters after their formation. Mars today is cold and dry, with no liquid water remaining stable for extended periods of time on the surface or in the atmosphere. However, many impact craters on the ancient Noachian surface units are highly degraded, suggesting that degradation rates were much higher early in Martian history [39] (Fig. 10). While a variety of geologic processes (including eolian deposition, volcanic lava flows, and impact cratering and ejecta deposition) were operating at higher rates during this early time period, analysis of how the topographic profile of these impact craters has been altered also suggests that rainfall and surface water flow were

responsible for much of the degradation during this time [40].

The presence of liquid water on the Martian surface during the planet's early history is problematic because temperatures on Mars, even with a thicker carbon dioxide-rich atmosphere, are expected to have been too low to support liquid water because the Sun is expected to have been fainter when the solar system first formed. However, numerical modeling of atmospheric effects from impacts into volatile-rich materials during this early period suggests that regional microclimates can be produced where excess greenhouse warming can allow conditions favorable for liquid water [41]. Valley network channels and alluvial fans within impact craters may have formed from such microclimate conditions.
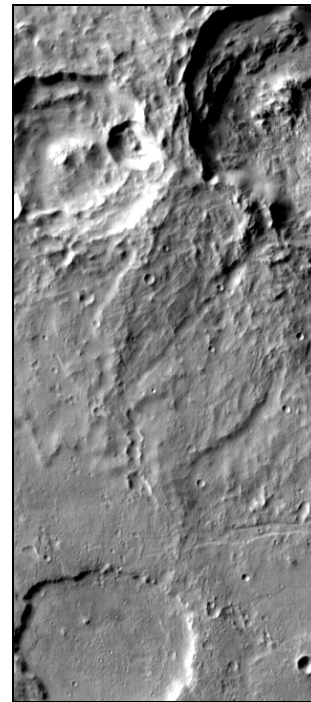

Figure 10: Example of the range of crater degradation seen in the ancient regions of Mars. Fresher craters, like that in the upper right, display prominent interior and ejecta features, while highly degraded craters, such as the one at the bottom, have had most of their features removed. Image is 32 km across and centered near 27°S 198°E. (THEMIS image I10579004)

The volatile-rich target affects impact craters in the mid-latitude regions of Mars through relaxation of crater topography, a process called "terrain softening" [42-44] (Fig. 11). The presence of ice in the target material weakens the crust, allowing relaxation of

22

topographic features over geologically short time periods. Sharp features such as crater rims and ejecta ramparts become rounded and material on steep slopes display features indicative of subsurface creep. Terrain softening is most common in the mid-latitude regions (~30°-60° latitude zone) because of the large presence of ice and the warmer temperatures which can be achieved in these regions due to seasonal and long-term obliquity cycles.

Figure 11: This 17-km-diameter crater shows features characteristic of terrain softening, caused by creep in target materials with high ice content. The rounded crater rim and ejecta features along with flow-type features on the crater floor are typical features seen in terrain softened craters on Mars. Crater is centered near 32°N 44°E (THEMIS image I11582007)

6. CONCLUSIONS

Martian impact craters display a variety of features which suggest that volatiles, both in the target material and the atmosphere, play a major role in crater formation and modification. Characteristics and distributions of the layered ejecta morphologies suggest that impact into volatile-rich surface materials is the dominant cause of these unusual features, although atmospheric interactions cannot be ignored as a contributor to the outermost ejecta deposit of double layer and multiple layer morphologies. Central pits are another strong indicator that the Martian near-surface region contains large concentrations of volatiles. Studies of onset diameters for single layer ejecta craters as a function of crater age suggest that the depth to the ice-rich layer has increased over time [45], but the deep reservoir seems to have maintained approximately the same volatile concentration for much of Mars' history [46].

Volatiles influence not only the initial morphologies and morphometries of Martian impact craters but also

their subsequent evolution. Ancient craters have undergone a substantial amount of degradation due to eolian, volcanic, tectonic, impact, and fluvial processes. Large impact events, particularly during the first 10^9 years of Mars' history, may have produced regional microclimates with enhanced fluvial and/or glacial activity. Present-day near-surface ice affects crater morphology through creep processes and sublimation of surface ice deposits emplaced at mid-latitudes during periods of high obliquity may be responsible for the unusual pedestal crater morphology.

Impact craters on Mars display numerous characteristics which differentiate them from craters on volatile-poor bodies like the Moon. Differences in impact velocities and surface gravity between Mars and the Moon can explain some of these observed differences, but many others must be the result of the volatile-rich Martian environment. The presence of both an atmosphere and surface/subsurface volatiles on the Earth makes Mars a better analog for understanding the original morphologies expected with terrestrial impact craters.

REFERENCES

1. Pike R. J., Control of crater morphology by gravity and target type: Mars, Earth, Moon, *PROCEEDINGS OF THE 11TH LUNAR AND PLANETARY SCIENCE CONFERENCE*, 2159-2189, 1980.
2. Davis P. A. and Soderblom L. A. Modeling crater topography and albedo from monoscipic Viking Orbiter imagers, 1, Methodology, *J. GEOPHYSICAL RESEARCH*, Vol. 89, 9449-9457, 1984.
3. Garvin J. B. et al. North polar region craterforms on Mars: Geometric characteristics from the Mars Orbiter Laser Altimeter, *ICARUS*, Vol. 144, 329-352, 2000.
4. Smith, D. E. et al. Mars Orbiter Laser Altimeter: Experiment summary after the first year of global mapping of Mars, *J. GEOPHYSICAL RESEARCH*, Vol. 106, 23,689-23,722, 2001.
5. Melosh, H. J., *Impact Cratering: A Geologic Process*, Oxford University Press, New York, 1989.
6. Garvin J. B. et al. Craters on Mars: Global geometric properties from gridded MOLA topography, *6th INTERNATIONAL CONFERENCE ON MARS*, Lunar and Planetary Institute Abstract #3277, Houston, TX, 2003
7. Rossbacher L. A. and Judson S. Ground ice on Mars: Inventory, distribution and resulting landforms, *ICARUS*, Vo. 45, 39-59, 1981.
8. Fanale F. P. Martian volatiles: Their degassing history and geochemical fate, *ICARUS*, Vol. 28, 179-202, 1976.

9. Clifford S. M. A model for the hydrologic and climatic behavior of water on Mars, *J. GEOPHYSICAL RESEARCH*, Vol. 98, 10973-11016, 1993.

10. Barlow N. G. et al. Standardizing the nomenclature of Martian impact crater ejecta morphologies, *J. GEOPHYSICAL RESEARCH*, Vol. 105, 26733-26738, 2000.

11. Carr M. H. et al. Martian impact craters and emplacement of ejecta by surface flow, *J. GEOPHYSICAL RESEARCH*, Vol. 82, 4055-4065, 1977.

12. Stewart S. T. et al. The relationship between rampart crater morphologies and the amount of subsurface ice, *LUNAR AND PLANETARY SCIENCE XXXII*, Abstract #2092, Lunar and Planetary Institute, Houston, TX, 2001.

13. Schultz P. H. Atmospheric effects on ejecta emplacement, *J. GEOPHYSICAL RESEARCH*, Vol. 97, 11623-11662, 1992.

14. Barnouin-Jha O. S. et al. Investigating the interactions between an atmosphere and an ejecta curtain. 2. Numerical experiments, *J. GEOPHYSICAL RESEARCH*, Vol. 104, 27117-27131, 1999.

15. Barlow N. B. and Perez C. B. Martian impact crater ejecta morphologies as indicators of the distribution of subsurface volatiles, *J. GEOPHYSICAL RESEARCH*, Vol. 108, #E08, 5085, doi: 10.1029/2002JE002036, 2003.

16. Kuzmin R. O. et al. Structural inhomogeneities of the Martian cryosphere, *SOLAR SYSTEM RESEARCH*, Vol. 22, 121-133, 1988.

17. Barlow N. G. et al. Variations in the onset diameter for Martian layered ejecta morphologies and their implications for subsurface volatile reservoirs, *GEOPHYSICAL RESEARCH LETTERS,* Vol. 28, 3095-3098, 2001.

18. Boyce J. M. et al. Distribution of onset diameters of rampart ejecta craters on Mars, *LUNAR AND PLANETARY SCIENCE XXVIII*, Abstract #1404, Lunar and Planetary Institute, Houston, TX, 1998.

19. Mouginis-Mark P. Martian fluidized ejecta morphology: Variations with crater size, latitude, altitude, and target material, J. GEOPHYSICAL RESEARCH, Vol. 84, 8011-8022, 1979.

20. Costard F. M. The spatial distribution of volatiles in the Martian hydrolithosphere, *EARTH, MOON, AND PLANETS*, Vol. 45, 265-290, 1989.

21. Barlow N. G. Sinuosity of Martian rampart ejecta deposits, *J. GEOPHYSICAL RESEARCH*, Vol. 99, 10927-10935, 1994.

22. Boynton W. V. et al. Distribution of hydrogen in the near-surface of Mars: Evidence for subsurface ice deposits, SCIENCE, Vol. 297, 81-85, 2002.

23. Feldmann W. C. et al. Global distribution of near-surface hydrogen on Mars, *J. GEOPHYSICAL RESEARCH*, Vol. 109, E09006, doi: 10.1029/2003JE002160, 2004.

24. Mitrofanav I. G. et al. Soil water content on Mars as estimated from neutron measurments by the HEND instrument onboard the 2001 Mars Odyssey spacecraft, *SOLAR SYSTEM RESEARCH*, Vol. 38, 253-257, 2004.

25. Boyce J. M. and Mouginis-Mark P. J. Martian craters viewed by the THEMIS instrument: Double-layered ejecta craters, *J. GEOPHYSICAL RESEARCH,* in press, 2006.

26. Barlow N. G. Impact craters in the northern hemisphere of Mars: Layered ejecta and central pit characteristics, *METEORITICS AND PLANETARY SCIENCE*, in press, 2006.

27. Barlow N. G. A review of Martian impact crater ejecta structures and their implications for target properties, in *Large Meteorite Impacts III* (T. Kenkmann, F. Hörz, and A. Deutsch, eds.), Geological Society of America Special Paper 384, 433-442, 2005.

28. Barlow N. G. and Bradley T. L. Martian impact craters: Correlations of ejecta and interior morphologies with diameter, latitude, and terrain, *ICARUS*, Vol. 87, 156-179, 1990.

29. McEwen A. S. et al. The rayed crater Zunil and interpretations of small impact craters on Mars, *ICARUS*, Vol. 176, 351-381, 2005.

30. Hartmann W. K. and Barlow N. G. Nature of the Martian uplands: Effect on Martian meteorite age distribution and secondary cratering, *METEORITICS AND PLANETARY SCIENCE*, in press, 2006.

31. Barlow N. G. and Hillman E. Distributions and characteristics of Martian central pit craters, *LUNAR AND PLANETARY SCIENCE XXXVII*, Abstract #1253, Lunar and Planetary Institute, Houston, TX, 2006.

32. Croft S. K. A proposed origin for palimpsests and anomalous pit craters on Ganymede and Callisto, *PROCEEDINGS OF THE 14TH LUNAR AND PLANETARY SCIENCE CONFERENCE, JOURNAL OF GEOPHYSICAL RESEARCH*, Vol.88, B71-B89, 1983.

33. Horner V. M. and Greeley R. Pedestal craters on Ganymede, *ICARUS*, Vol. 51, 549-562, 1982.

34. Schenk P. H. Central pit and dome craters: Exposing the interiors of Ganymede and Callisto, *J. GEOPHYSICAL RESEARCH,* Vol. 98, 7475-7498, 1993.

35. Moore J. M. et al. Impact features on Europa: Results of the Galileo Europa Mission (GEM), *ICARUS*, Vol. 151, 93-111, 2001.

36. Wood C. A. et al. Interior morphology of fresh Martian craters: The effects of target characteristics, *PROCEEDINGS OF THE 9TH LUNAR AND PLANETARY SCIENCE CONFERENCE*, 3691-3709, 1978.

37. Pierazzo E. et al. Starting conditions for hydrothermal systems underneath Martian craters: Hydrocode modeling, in *Large Meteorite Impacts III* (T. Kenkmann, F. Hörz, and A. Deutsch, eds.),

Geological Society of America Special Paper 384, 443-457, 2005.

38. Klaybor K. M. and Barlow N. G. Interior morphologies of impact craters on Ganymede, *LUNAR AND PLANETARY SCIENCE XXXVII*, Abstract #1360, Lunar and Planetary Institute, Houston, TX, 2006.

39. Chapman C. R. and Jones K. L. Cratering and obliteration history of Mars, *ANNUAL REVIEWS OF EARTH AND PLANETARY SCIENCE*, Vol. 5, 515-540, 1977.

40. Craddock R. A. and Howard A. D. The case for rainfall on warm, wet early Mars, *J. GEOPHYSICAL RESEARCH*, Vol. 107, No. E11, 5111, doi: 10.1029/2001JE001505, 2002.

41. Colaprete A. et al. The effect of impacts on the Martian climate, *WORKSHOP ON THE ROLE OF VOLATILES AND ATMOSPHERES ON MARTIAN IMPACT CRATERS*, LPI Contribution No. 1273, Lunar and Planetary Institute, Houston, TX, 32-33, 2005.

42. Squyres S. W. and Carr M. H. Geomorphic evidence for the distribution of ground ice on Mars, *SCIENCE*, Vol. 231, 249-252, 1986.

43. Jankowski D. G. and Squyres S. W. The topography of impact craters in "softened" terrain on Mars, *ICARUS*, Vol. 100, 26-39, 1992.

44. Turtle E. P. and Pathare A. V. "Softening" of Martian impact craters by creep of ice-rich permafrost, *WORKSHOP ON THE ROLE OF VOLATILES AND ATMOSPHERES ON MARTIAN IMPACT CRATERS*, LPI Contribution No. 1273, Lunar and Planetary Institute, Houston, TX, 110-111, 2005.

45. Reiss D. et al. Ages of rampart craters in equatorial regions on Mars: Implications for the past and present distribution of ground ice, *METEORITICS AND PLANETARY SCIENCE*, in press, 2006.

46. Barlow N. G. Martian subsurface volatile concentrations as a function of time: Clues from layered ejecta craters, *GEOPHYSICAL RESEARCH LETTERS*, Vol. 31, L05703, doi: 10.1029/2003GL019075, 2004